Surface Hydration and Cationic Sites of Nanohydroxyapatites with Amorphous or Crystalline Surfaces: A Comparative Study

UNIVERSITÀ DEGLI STUDI DI TORINO

Surface hydration and cationic sites of nanohydroxyapatites with amorphous or crystalline surfaces: a comparative study

Yuriy Sakhno[a], *Luca Bertinetti*[a], *Michele Iafisco*[b,c], *Anna Tampieri*[d], *Norberto Roveri*[b], *and Gianmario Martra*[a,*]

[a]Dipartimento di Chimica IFM & Centro di Eccellenza Interdipartimentale "NIS", Università di Torino, Via P. Giuria 7, 10125 Torino - Italy

[b]Dipartimento di Chimica "G. Ciamician", Università di Bologna, Via Selmi 2, 40126 Bologna – Italy

[c]Dipartimento di Scienze Mediche, Università del Piemonte Orientale, Via Solaroli 4, 28100 Novara, Italy

[d] ISTEC-CNR, Via Granarolo 64, 48018 Faenza - Italy

*Corresponding author. Fax: +39-011 670 7855; Tel: +39-011 670 7538. E. mail: gianmario.martra@unito.it

Abstract

This paper is an extension of previous work devoted to the characterization of platelet-like hydroxyapatite (HA) nanoparticles constituted by a crystalline core coated by an amorphous surface layer 1 to 2 nm thick (L. Bertinetti et al. J. *Phys. Chem C.* 2007, *111*, 4027–4035). By increasing the preparation temperature, the platelet morphology was retained but HA nanoparticles exhibited a higher degree of crystallinity (evaluated by X-ray diffractometry). High resolution transmission electron microscopy revealed that in this case the crystalline order was extended up to the particles surfaces, that were of the (010), (100) and (001) types. IR spectroscopy was used to investigate the surface hydration of both materials, in terms of adsorbed H_2O molecules and surface hydroxy groups, as well as the Lewis acidity of surface cations, by removing water and adsorbing CO. For both features, strong similarities between amorphous and crystalline surfaces were found.

Keywords: nanohydroxyapatites, surface structure, adsorbed water, surface cations, HR-TEM, IR spectroscopy of adsorbed molecules.

1. Introduction

Most improvements/innovations achieved in the last decades in the field of biomaterials derived from a growing awareness of the major role played by the physico-chemical features of the surface, *i.e.* the biomaterial region actually in contact with the host biological environment. This led to the definition of the concept of "biological/biomedical surface science", which, at the beginning of the 2000s, was recognized as one of the frontiers of surface science.[1-3] A great deal of research has been carried out in this respect, mainly devoted to the investigation of "average" surface properties, such as wettability and surface charges, that are commonly used to assess surface adhesion through DLVO calculations.[4] Still, a better understanding on a more detailed scale, down to the atomic/molecular level, is needed, since the causal sequence biomaterial surface structure/states of adsorbed water/states of adsorbed proteins has been recognized. [1-3,5,6] This was also the origin of the interest in disclosing preparation-conditions/surface-structure (and reactivity) relationships, in order to try to rule the interaction with biomolecules, that represents the first, fundamental step of the biomaterials/host tissues dialog.

Among inorganic biomaterials, biomimetic hydroxyapatites (HA), attracted attention since long time as bioactive bioresorbable bone substitute, and it has been the subject of an intense research activity,[7] also aimed at finding materials and preparation procedures that would result in the exposure of surfaces with optimized properties. [8-11] In this respect, relevant advances in the elucidation of HA surface structure-properties relationships were obtained for micrometric hydroxyapatite particles terminated by defined crystal planes (calcium hydroxyapatite belongs to the $P6_3/m$ space group), that exhibited two families of different binding sites, called C and P sites, respectively.[12] C sites, arranged in a rectangular array on *ac* or *bc* faces and rich in calcium ions, should act as adsorbing sites for acidic proteins, whereas P sites, arranged hexagonally on the *ab* faces and lacking calcium ions, are expected to behave as adsorbing sites for basic proteins. Furthermore, the presence of calcium ions in highly regular, repeating surface geometries was proposed to be a key factor in hydroxyapatite surface-induced peptide-

folding,[13] and detailed insights into the structure of crystalline HA surfaces and their interaction with water and amino acids were provided by modeling.[14]

Evolution in the preparation techniques has led to methods for obtaining HA in nanosized forms, mimicking those naturally occurring in bone.[15,16] Interestingly, nano-HA exhibited improved *in vitro* performances in tests with osteoblasts.[17] Structure is also important for biomimetism, as the mineral component of bone has well defined features in relation to bone tissue function and age.[18,19] In this respect, the possibility to turn quite smoothly the bulk structure from highly to poorly crystalline or actually disordered by changing preparation conditions such as temperature, presence of anionic and/or cationic substituents, nucleation on collagen fibers, is well known.[20]

Still, in recent years, several studies, carried out by spectroscopic methods (solid-state NMR, IR, X-ray absorption)[21-23] and high resolution transmission electron microscopy (HR-TEM),[24] revealed that HA nanoparticles, also doped with B,[25] can be coated by an amorphous, non-apatitic surface layer surrounding a crystalline hydroxyapatite bulk. It is of interest to note that in an NMR study of the mineral–protein binding in bone, [26] it was found that the binding carboxyl resonance was very broad reflecting the disordered nature of the apatite mineral phase at the surface.

However, the possibility to obtain apatitic particles with crystalline structure extended up to the surface was reported for Ca^{2+}/Mg^{2+} apatites.[27] Nevertheless, in that case the borders of nanoparticles appeared quite irregular, indicating that no specific crystalline planes were exposed at their surfaces.

Recently, some of us set up a method to obtain well shaped, highly crystalline nano-HA,[28] and this materials appeared an ideal candidate for a comparative study between crystalline HA surfaces and amorphous ones, that have been the subject of a previous work.[24] Main targets were the study of adsorbed water molecules, that are the ligands that biomolecules should displace to interact directly with the biomaterial surface, and cationic sites, which are the adsorbing centers for negative groups exposed by biomolecules, typically carboxylate groups.[14]

To this aim, high resolution transmission electron microscopy was used to highlight the level of structural order of the surfaces, while adsorption behavior towards water and Lewis acidity of surface cations were investigated by IR spectroscopy of adsorbed H_2O and CO, respectively.

2. Experimental

2.1. Materials

The hydroxyapatite powders were synthesized using an aqueous medium procedure by dropping a solution of H_3PO_4 (1.26 M, 0.6 L) into a $Ca(OH)_2$ suspension (1.35 M, 1.0 L), to accomplish the following reaction: $5Ca(OH)_2+3H_3PO_4 \rightarrow Ca_5(PO_4)_3OH+9H_2O$.

The reaction mixtures were stirred under N_2 atmosphere for 24 hours. In one case the temperature was 313 K (the resulting material will be referred to as HA-am, because of the presence of a surface amorphous layer), whereas in the other case the temperature was 368 K (the resulting material will be referred to as HA-cry, because crystalline up to the surface).

The stirring was then suspended and the mixtures were left standing for 2 hours to allow for deposition of the inorganic phase. The HA powders were then isolated by filtration of the mother liquor, repeatedly washed with water and dried at room temperature.

For IR measurements, high purity CO (Praxair) was employed without any additional purification except liquid nitrogen trapping, whereas H_2O and D_2O (99.9 at.% D, Aldrich) were admitted onto the samples after several freeze-pump-thaw cycles.

2.2. Methods

Specific surface area (SSA) was measured with a Micromeritics ASAP 2010 by nitrogen adsorption at 77 K following the BET model. The Ca/P ratio was determined by inductively coupled plasma-optical emission spectrometry (ICP-OES, Liberty 200, Varian). Samples were dissolved in 1 wt % ultrapure nitric acid. The following analytical wavelengths chosen were 422 nm for Ca and 213 nm for P. Carbonate content was evaluated on dried samples by thermogravimetric analysis (TGA) investigations using a Thermal Analysis SDT Q 600 (TA Instruments). X-ray diffraction (XRD) pattern of the powders were recorded with a Analytical X'Pert Pro equipped with an X'Celerator detector powder diffractometer using Cu Ka radiation generated at 40 kV and 40 mA. The instrument was configured with 1/2° divergence and receiving slits. A quartz sample holder was used. The 2θ range was from 5° to 60° with a step size (°2θ) of 0.05 and a counting time of 3 s.

The degree of HA crystallinity was calculated according to the formula:[28]

$$Crystallinity[\%] = 100 \cdot \frac{C}{(A+C)}$$

where C was the area from the peaks in the diffraction pattern ("the crystalline area") and A was the area between the peaks and the background ("the amorphous area").

Crystal domain size along the HA axis directions were calculated applying the Scherrer equation:[29]

$$L_{(hkl)} = \frac{0.94\lambda}{\left[\cos\theta(\sqrt{\Delta r^2 - \Delta_0{}^2})\right]}$$

where θ is the diffraction angle for plane (hkl), Δr and Δ_0 the widths in radians of reflection (hkl) at half height for the synthesized and pure inorganic hydroxyapatite (Standard reference material, Calcium Hydroxyapatite, National Institute of Standards& Technology), respectively, and λ=1.5405 Å.

High resolution transmission electron microscopy (HR-TEM) images of the materials (powder grains dispersed on lacey carbon Cu grids) were obtained using a JEOL 3010-UHR with an acceleration potential of 300 kV. As apatite samples might evolve under the electron beam, potentially leading to further crystallization and/or loss of bulk water,[20,30,31] observations were carried out under low

illumination conditions (significantly lower than that indicated in the references) to avoid any modifications to the materials during the analysis.

To prepare for IR study of the surface, the powders were pressed in self-supporting pellets and placed in a quartz IR cell equipped with CaF_2 windows designed to carry out spectroscopic measurements both at beam temperature (b.t.; ca. 323 K) or at low temperature (ca. 100 K, by cooling with liquid N_2). The cell was connected to a conventional vacuum line (residual pressure: 1×10^{-5} mbar, 1 mbar=10^2 Pa) allowing all thermal treatments and adsorption–desorption experiments to be carried out *in situ*. A Bruker Vector 22 spectrometer (resolution: 4 cm^{-1}; detector: DTGS) was employed for the spectra collection. The data were normalized to the intensity of a pattern in the 2200-1900 cm^{-1} range due to a combination and overtone of vibration modes of bulk phosphate groups in order to render differences in intensity independent of differences in the thickness of the pellets. For comparative analysis of the intensity of surface species, some spectra were also normalized with respect to SSA.

Finally, in the case of the spectra of adsorbed CO, the spectrum of the sample before CO admission was subtracted as a background.

3. Results and discussion

3.1 Compositional, textural and structural features of HA-am and HA-cry

3.1.1. Global Characterization

Codes, composition and specific surface area (SSA) of the investigated materials are listed in Table 1. In both cases, the Ca/P ratio was slightly lower than the stoichiometric one (1.67), and a limited amount of carbonate groups, derived from unintentionally dissolved CO_2 in the preparation media and from CO_2 adsorbed onto the surface materials during the storage, was present.

As for texture, both materials exhibited an SSA in the 70-80 $m^2 \cdot g^{-1}$ range, which is in agreement with the nanometric size observed by TEM (see next section).

Please, insert here Table 1

General structural insights were obtained from the XRD patterns (Supporting Information, Fig. S1), which show the characteristic diffraction maxima of hydroxyapatite single phase (JCPDS 9-432). The diffraction pattern of HA-am exhibits not well defined diffraction maxima indicating a relatively low degree of crystallinity. In contrast, HA-cry exhibits a higher degree of crystallinity resulting from the higher temperature of synthesis (368 K). The degree of crystallinity of HA-am and HA-cry was 70 % ± 3 and 83 % ± 4, respectively, and differed significantly (p-value<0.0001). The crystal domain sizes along the *c*-axis (D_{002}) and along a perpendicular to it (D_{310}), were calculated using Scherrer's formula using the 2θ = 26° (002) and 2θ = 39° (310) diffraction peaks, respectively (Table 1). The crystallite domain sizes of the nanocrystals synthesised at lower temperature (HA-am) appeared slightly shorter than the domain sizes of HA-cry.

3.1.2. Morphology and surface structure: HR-TEM observations

The second step in the characterization of the two types of HA powders was aimed at describing their morphological, structural and surface features by HR-TEM. Images representative of the two materials are displayed in Figures 1 and 2. Both of them appeared to be constituted by primary nanoparticles, stacked on each other, mainly along their length, to form agglomerates (Fig. 1). In the case of HA-am, primary particles appeared 50-150 nm long and 10-70 nm width (Fig. 1A); the thickness in the direction normal to the image plan was evaluated through the simulation by a Bloch wave functions approach (EMS Online) of high resolution images,[24] and was also found to be of 20-40 nm. As for the HA-cry material (Fig. 1B), many particles exhibited, projected in the image plan, an almost platelet squared shape with sides ranging from 40 to 100 nm. In other cases, particles appearing acicular in the image plane, with length in the 40-100 nm range and width of 5-10 nm were observed, exhibiting a much higher contrast. Such projected shapes should correspond to a "side" view of platelets lying perpendicularly to the to the image plane. It can be then concluded that both materials exhibit a platelet like morphology, with dimensions (length × width × thickness) of ca. 50-150 × 10-70 × 20-40 nm in the case of HA-am and of 40-100 × 40-100 × 5-10 nm for HA-cry. Hence, HA-am particles appeared more elongated in one direction (coincident with the *c*-axis, along the [001] direction, *vide infra).*

The size of the particles measured by TEM appeared larger than the size of crystal domains calculated from XRD (Table 1), and this discrepancy can be rationalized by considering that:

i) The HA materials considered are not completely crystalline, and the difference between TEM and XRD data increases with the decrease in crystallinity.

ii) The presence of impurities (i.e. carbonate ions) and deviations from ideal stoichiometry contribute to the shortening of the coherency domains.

iii) TEM allows to determine only ranges of values, while by XRD average values are obtained.

Nevertheless, the aspect ratio of the crystal domains (D_{002}/D_{310}) calculated from XRD follows the trend in the aspect ratio of the particles measured by TEM (length/width).

Please, insert here Figure 1

Observations in high-resolution conditions provided insights into the bulk and surface structure of the materials. Figure 2A, for example, shows a particle of HA-am observed from the [2,0,1] zone axis (as from the FT pattern in the right part of Fig. 2A). First of all, the presence of interference fringes observed over the particle indicated that the material has a crystalline core. Then, from the analysis of the phase contrast, the orientation of the crystallographic axes with respect to the image plane was retrieved so that the direction of elongation of the particles was found to be coincident with the c-axis of the HA lattice. However, as reported in previous work[24] the crystal order does not extend up the boundary of the particle; the phase contrast due to the lattice plans of the crystal vanishes near the surface and is replaced by a region 1 to 2 nm thick exhibiting a contrast typical of an amorphous region (Fig. 2A, zoomed view of insets A',A''). The amorphous layer was the origin of the "HA-am" code for this material. Finally, the particle exhibits quite curved borders, whereas no flat edges could be recognized. It is important to stress here that, although the material is actually hydroxyapatite, its surface is not exactly a "hydroxyapatite surface", and instead of regular pattern of ions characterized by translational symmetry, a random arrangement of cationic and anionic sites should be expected.

Please, insert here Figure 2

In Figure 3 details in high resolution of two HA-cry nanoparticles are reported. It can be clearly seen that an amorphous layer is not present in this case, as the phase contrast in the HR-TEM images of this latter (see also the zoom of insets A,A'') extends up to the boundary of the image, indicating that the crystalline order reached the particle surface, where regular patterns of calcium and phosphate should be exposed (from here the "HA-cry" code for this material) . Furthermore, the two images offer a complementary view of a typical platelet crystal of HA-cry. For the particles in Fig. 3A, the a- and c-axis

(sample observed along the [010] zone axis) lye in the image plane. In the case of the particle in Fig. 3B the same is true for the b-axis, whereas a ca. 20° angle exists between the c-axis and the image plane (sample observed along the [201] zone axis). Under these conditions, the extension along the crystallographic axes can be directly estimated from the elongation of the particle in the corresponding direction in the image plane. Thus, the directions of extension for HA-cry are the a- and c-axes. Considering, furthermore, that the phase contrast of the image of HA-cry observed along the [010] zone axis is rather homogeneous, which indicates a constant thickness of the material in the direction perpendicular to the image plane, it is possible to conclude that HA-cry nanocrystals expose extended (010) surfaces while those of the (100) and (001) types are quite limited. It is of interest to note that these latter surfaces appeared (almost) atomically flat (Fig. 3, zooms of insets A',A''), while the (010) exhibited some sub-nanometric steps (Fig. 3B).

Please, insert here Figure 3

3.2 Hydration surface species. IR investigations

3.2.1 Study of thermally untreated materials

Figure 4 shows the spectra of HA-am (panel A) and HA-cry (panel B) in the presence of 20 mbar of H_2O vapor (curves a), after outgassing at beam temperature (b.t.; curves b) and after the final outgassing at the end of a series of D_2O adsorption/desorption cycles (curves c).

Please, insert here Figure 4

The low frequency side of the displayed spectral range was limited to 1350 cm^{-1}. This value is the onset of the cut-off due to the fundamental absorptions of the lattice phosphate groups. The two materials exhibited similar spectral patterns that, on the basis of the previous study devoted to HA-am,[24] are assigned as follows:

i) Overtone and combination modes of the fundamental phosphate absorptions produced the 2200-1900 cm^{-1} weak pattern. Another signal due to bulk species is the sharp peak at 3570 cm^{-1}, due to the stretching of OH^- groups occupying the 4e position in the hexagonal lattice of HA, and arranged to form like "columns" in the bulk. The set of components in the 1550-1350 cm^{-1} range is related to the stretching modes of carbonate groups.[32-34] Such components exhibited some change in shape and relative intensity that was dependent on the amount of adsorbed water (see also the insets in the two panels), indicating that part of the carbonate groups were located at the surface. In particular, the modification occurred to a larger extent for HA-cry, which should then expose higher amounts of surface carbonates.

ii) Adsorbed water molecules were responsible for the band at 1642 cm^{-1} (bending mode, δH_2O) and of most part of the complex absorption in the 3500-2500 cm^{-1} range, resulting from the superposition of the in-phase and out-of-phase H_2O stretchings bands as well as the stretching of surface and bulk hydroxy groups involved in H-bonding. Passing from the presence of 20 mbar of water vapor (curves a) to vacuum (by outgassing at b.t., curves b) the amount of adsorbed H_2O was decreased from a multilayer state (also exposing dangling –OH, responsible for the very weak signal at 3695 cm^{-1}) to an hydration layer constituted by single molecules left adsorbed on surface cations through a coordinative interaction.

iii) After subsequent exchange with D_2O followed by outgassing at b.t. (curves c), a weak component due to the bending mode of water molecules entrapped in the bulk was observed for both materials. The stretching modes of these molecules contributed to a part of the broad and asymmetric absorption spread over the 3500-2500 cm^{-1} range, which contained the signal due to bulk hydroxy groups involved in hydrogen bonding as well. The broad band in the 2800-2000 cm^{-1} range was due to the stretching mode

of surface –OD groups and adsorbed D_2O molecules, while band related to the bending mode of these latter, expected at ca. 1200 cm^{-1}, was outside the transparency window of the materials.

By considering the shape of the complex absorptions due to the stretching modes of H_2O molecules and hydroxy groups, it can be observed that, when dominated by the contributions due to surface species (curves a,b), in the case of HA-am the profile appeared broadened towards the low frequency side (Fig. 4A), indicating the presence of a larger amount of O-H oscillators involved in stronger H-bonding. Vice-versa, no significant differences were observed for the ν_{OH} profiles related to bulk water and hydroxy groups (curves c). Furthermore, the comparison of the intensity of the δH_2O bands in the normalized spectra after exchange with heavy water indicated equivalent amounts of water molecules entrapped in the bulk of the two materials (Supporting Information, Fig. S2).

The slightly higher intensity of the ν_{OH} band in the 3500-2500 cm^{-1} range observed in the case of HA-cry should be then due to some difference in the amount of bulk H-bonded hydroxy groups. In the previous work devoted to the investigation of HA-am, such species were tentatively associated to the presence of the amorphous surface layer. Based on the present results, this hypothesis could hold if the H/D exchange proceeded to some extent also in the amorphous layer as well. This possibility, and/or alternative explanations, will be considered in a future paper.

The next step in analyzing the spectra was the attainment of a quantitative comparison between the surface hydration of the two materials. To this aim, the spectra obtained after exchange with D_2O and subsequent outgassing (curves c) were subtracted as a background from those recorded in the presence of 20 mbar of water vapor (curves a) and after outgassing at b.t. (curves b). This process produced patterns that contained only signals due to surface hydration species, i.e., water molecules and hydroxy groups. An example of the adopted procedure is reported in the Supporting Information, Fig. S3A, also showing how the appearance of a negative contribution in the νOD range was avoided. The spectra of the two materials were normalized to both the intensity of the 2200-1900 cm^{-1} pattern due to overtone and combination modes of bulk phosphates (to refer the spectra to the same amount of sample) and to the specific surface area (to refer to the spectra to the same surface extension) so that in the resulting

spectra (displayed in Supporting Information, Fig. S3B), differences in intensity should reflect actual differences in the amount of surface hydration species. The values of the integrated intensity of the bands resulting from the subtraction procedure indicated above are listed in Table 2.

Please, insert here Table 2

Because the δH_2O bands in the 1750-1550 cm^{-1} range were due to H_2O only, their integrated intensity was unequivocally related to the amount of adsorbed water molecules. In a previous study on HA-am, the combination of IR and microgravimetric data allowed for evaluation of the amount of H_2O molecules left coordinated to surface cations after outgassing at b.t. (ca. 4.5/nm^2).[24] Then, the proportionality between the number of water molecules per surface unit and the integrated intensity of the δH_2O band was established. On this basis, the amount of water adsorbed in multilayers (in the presence of 20 mbar of H_2O vapor) or left coordinated to surface cations after outgassing at b.t. was evaluated, and the obtained results are listed in Table 3 (entries 1,2). It is of interest to note that coverage of ca. 4.5 H_2O molecules per nm^2 should correspond to the occupancy of each surface Ca^{2+}ions by one water molecule.[24]

Please, insert here Table 3

By considering the incertitude of the values, the capability of the two materials to adsorb H_2O up to the formation of multilayers appeared essentially equivalent (entry 1), whereas the amount of water molecules retained on surface Ca^{2+} ions after outgassing at b.t. was found to be slightly lower in the case of HA-cry (entry 2). It can be proposed that such a decrease resulted from the involvement of some cations in the stabilization of surface carbonates groups that are more abundant for this latter material (Fig. 4 and related comment).

Analysis of the broad signal in the 3500-2500 cm^{-1} range was less straightforward because of the superposition of the νOH components due to adsorbed water molecules and surface hydroxy groups involved in H-bonding. However, some evaluation was attempted to focus on the profiles related to the samples outgassed at b.t. The decreased amount of adsorbed water allowed for an easier and more consistent detection of possible differences related to the content of the surface hydroxy groups (not desorbed after such a treatment) in the two materials. Actually, the ratio between the integrated area of the νOH (due to both surface hydroxy groups and adsorbed H_2O molecules) and δH_2O (due to water molecules only) resulted in a lowering by ca. 20% in the case of HA-cry (Table 2, last column). This indicates that on the crystalline surfaces hydroxy groups involved in H-bonding are less abundant. In particular, because in the case of HA-am, the integrated intensity of the νOH band corresponded to the presence of 4.5±0.5 H_2O molecules and 0.9±0.2 surface H-bonded –OH per nm^2,[24] it can be deduced that on HA-cry, retaining 3.7±0.5 H_2O molecules per nm^2 (see Table 2), ca. 0.6±0.3 surface H-bonded –OH per nm^2 should be present.

3.2.2 Study of materials outgassed at increasing temperature and rehydration

To compare the features of cations exposed by HA-am and HA-cry by IR spectroscopy of adsorbed CO, the removal of H_2O molecules left coordinated to surface Ca^{2+} after outgassing at b.t. was required. The two materials were then outgassed at increasing temperatures, taking into account that the previous study on HA-am revealed that such treatments resulted also in a modification of the surface structure that affected their capability to reabsorb water.[24] Thus, a stepwise outgassing of HA-cry was carried out and, once the spectrum was recorded, the sample was contacted with H_2O and then outgassed at b.t. to check the level of rehydration. As in the case of HA-am,[24] a linear relationship between the integrated intensity of νOH and δH_2O bands growing by admission of progressive small doses of water vapor on

HA-cry pre-outgassed up to 573 K was found (Supporting Information, Fig. S4). This indicated that water readsorption at b.t. was essentially molecular in nature, without restoration of hydroxy groups.

Subsequently, a surface H/D exchange was performed by of admission/outgassing of D_2O. This shifted the bands due to surface hydration species and allowed us to monitor the evolution of bulk water molecules and H-bonded hydroxy groups. Furthermore, the obtained spectral patterns were used as background for subsequent elaboration of the data (as done for the spectra commented on in the previous section). Finally, before proceeding to the next outgassing step, the sample was back-exchanged with H_2O by contact with 20 mbar of H_2O vapor, and then outgassed at b.t..

The results obtained for HA-cry, reported in Fig. 5, are divided into three sections in order to allow use of the most appropriate scales for each range of interest. For HA-am, this type of data, limited to two regions, was reported in previous paper.[24] Here, such data set, completed with the third range, is shown in Supporting Information, Fig. S5.

Please, insert here Figure 5

The collection of spectra dealing with HA-cry indicated that both bulk and surface water molecules and H-bonded hydroxy groups were completely removed by outgassing up to 573 K , as proved by the flatness of the spectra in the 3500-2500 cm^{-1} νOH range(Fig. 5A) and δH_2O region (Fig. 5B). Similar behavior was exhibited by surface PO-H not involved in H-bonding, which was responsible for the very weak signal at ca. 3660 cm^{-1}.[24,35] Finally, the bands due to carbonate groups exhibited a progressive evolution (Fig. 5C), and progressively lost their sensitivity to the presence/absence of multilayers of water (Supporting Information, Fig. S6), indicating the depletion of surface carbonate groups.

Then, the relative extent of the desorption of water molecules, depending on the outgassing temperature, was calculated for both materials on the basis of the integrated area of the δH_2O band (I δH_2O), and HA-cry appeared slightly more resistant to dehydration than HA-am (Fig. 6).

Please, insert here Figure 6

The back-exchange with H_2O after deuteration allowed us to monitor the reversibility of the dehydration at each outgassing step. Then, the integrated intensity of the δ_{H2O} bands, resulting from the contact with 20 mbar of water vapor (H_2O multilayers) and subsequent outgassing at b.t. (H_2O left adsorbed on surface cations), were computed (spectra in Supporting Information, Fig. S7) and plotted in dependence on the pre-outgassing temperature as a percentage of the $I\delta H_2O$ obtained in the two hydration conditions for the original, thermally untreated materials (Fig. 7).

Please, insert here Figure 7

Both materials exhibited a similar loss of capability to coordinatively re-adsorb water on surface cations, that after pre-outgassing at 573 K resulted in only 45-50% of the initial one (Fig. 7A). The amount of H_2O molecules in interaction with surface Ca^{2+} sites appeared equivalent now for the two materials (Table 3, entry 4), likely as a consequence of the removal of surface carbonate groups that were more abundant on HA-cry (see above), and a similar evolution of the surface cationic sites in both cases. Such a loss in the capability to re-adsorb H_2O on surface cations should be the result of some change in the surface structure of the materials. This change was previously proposed to involve some downward relaxation of initially exposed Ca^{2+} ions.[24] Actually, a recent theoretical work on H_2O adsorption on HA indicated that any relaxation should occur for ideal, stoichiometric (001) and (010) surfaces.[36] However, it can be considered that the actual surface composition (including carbonates and OH groups, progressively removed by outgassing at increasing temperature) and structure (amorphous layer for HA-am, stepped (010) surfaces for HA-cry) might have played a role.

A remarkable feature is represented by the evolution of the capability of the two materials to reabsorb water in multilayers after pre-outgassing at increasing temperature (Fig. 7B). For HA-am, it dropped ca.

35%, whereas for HA-cry the decrease was limited to ca. 10%, resulting in significantly higher levels of hydration that were finally exhibited by this latter material (Table 3, entry 3). These two different behaviors suggest that the possibility of building up H_2O multilayers is not simply dependent on the extension of the "first hydration layers" but also on the reciprocal location of H_2O molecules coordinated to surface cations, that is expected to be disordered on HA-am and ordered on HA-cry. To elucidate this point, studies aimed to assess the structural features of water adsorbed at different coverages on the two types of surfaces are in progress. Extension of the spectroscopic investigation to the NIR range, where spectral features highly sensitive to the H-bond networking among water molecules can be observed,[27] is also being studied.

3.3 Features of surface Ca^{2+} probed by IR spectroscopy of CO adsorbed at 100 K

The third part of the investigation was devoted to the comparison of the features of Ca^{2+} ions exposed at the surface of HA-am and HA-cry after removal of water molecules using CO as a vibrational probe. Namely, carbon monoxide was adsorbed (at low temperature, ca. 100 K, in order to allow for interactions with surface sites with a weak Lewis acid strength[37]) on HA-am (HA-cry) pre-outgassed at two temperatures: i) 403 (433) K, the best compromise between a high extent of water removal from the cationic sites (see Fig. 6) and a limited surface modification (see Fig. 7A); and ii) 573 K, where a more severe surface modification occurred (Fig. 7A), but the removal of water molecules and surface carbonate groups was complete (Fig.s 5 and 6).

The spectra (νCO region) obtained for decreasing coverage of CO adsorbed on the two samples, which were pre-outgassed at the indicated temperatures, have been composed in Fig. 8.

Please, insert here Figure 8

In all cases, a broad band, initially located at ca. 2170 cm^{-1} and then shifting, while decreasing in intensity, to ca. 2180 cm^{-1} was observed, which was related to CO molecules adsorbed on surface Ca^{2+}, with a possible very weak contribution from CO adsorbed on surface P-OH .[24,38] The progressive upward shift in position should result from both adsorbate-adsorbate interactions,[37] and the presence of components, rather close in frequency, due to CO adsorbed Ca^{2+} with different Lewis acidity, that resulted in a different reversibility and ν_{CO} of probe molecules interacting with them. The first features indicated that surface cations are not isolated from each other, and the second monitored the presence of some heterogeneity in the local structure of surface cations. This latter feature was better evidenced by calculating the second derivative of the νCO spectra[39] (Fig. 9; note that the direction of the lettering is reversed with respect to original spectra in Fig. 8, and then CO coverage decreases from the bottom to the top of each panel).

Please, insert here Figure 9

Actually, the resulting patterns exhibited a series of two ν_{CO} components, one shifting from 2168-2171 to ca. 2173-2174 cm^{-1} and the other from ca. 2178 to 2180-2181 cm^{-1}, which monitored the presence of two families of surface Ca^{2+} sites, exhibiting a weaker and stronger Lewis acidity, respectively. A similar pattern was also recently reported for another type of HA but without complementary information on the surface structure.[38]

On the basis of the profiles of the direct spectra in Fig. 8, weaker Lewis sites responsible for the component at ca. 2170 cm^{-1} appeared the most abundant in all cases, whereas the relative amount of stronger Lewis acid Ca^{2+} ($2181 \geq \nu CO \geq 2178$ cm^{-1}) seemed to be higher on HA-cry pre-outgassed at 433 K (Fig. 8B) and HA-am pre-outgassed at 573 K (Fig. 8A'). However, the similarities among the four sets of curves in Fig. 8 seemed to prevail on slight differences by far. The collection of all data allows us to conclude that both materials appeared quite similar in terms of the Lewis acidity of surface cations, at both pre-outgassing temperatures considered.

The last aspect to be considered is the intensity of the spectra of adsorbed CO, which, after normalization with respect to both the mass of each sample ("internal" standard: pattern in the 2200-1900 cm^{-1} spectra of the samples before CO adsorption) and the specific surface area, appeared essentially equivalent in all the four cases considered (Fig. 8). The rationalization of the invariance of the intensity of the ν_{CO} pattern observed for each material pre-outgassed at different temperatures is not straightforward, as it is in conflict with the significant decrease in the capability to adsorb H_2O molecules in terms of the "first hydration layer", which suggested the presence of lower amount of cations exposed at the surface after pre-outgassing at 573 K (see Fig. 7A, and Supplementary Information, Fig. SIR6). Furthermore, both types of molecules should have been able to probe all accessible surface cations. In the case of CO, this possibility should be guaranteed by the low temperature of adsorption. In the case of H_2O, adsorbed and desorbed at room temperature, this should be guaranteed by the strength of the interaction.[36] However, it can be proposed that the difference in the strength between H_2O and CO as ligands could have played a relevant role in some modification of the surface during the adsorption, as proposed in previous work on HA-am. By outgassing at 403/433 K, modification of the local structure of a relevant part of surface Ca^{2+} occurred to an extent large enough to render them unable to adsorb a weak probe molecule as CO. Such modification might be reversed by interaction with H_2O, which is definitely stronger than CO as ligand, and the, in rehydration tests water molecules probed the presence of a larger amount of surface Ca^{2+} sites. Pre-outgassing at 573 K resulted in a much more severe modifications of the local structure of several surface cations, likely irreversible by subsequent dehydration, and then these sites could no longer be probed by CO or H_2O.

4. Conclusions

The investigation carried out here highlights that it is possible to address the structure of surface terminations of hydroxyapatite nanoparticles to be amorphous or crystalline by properly selecting the preparation parameters and, in particular, the temperature.

The two types of surfaces appeared quite similar in term of their first hydration layer, as well as Lewis acid strength of exposed Ca^{2+} ions. Both features have a strong dependence on the local structure of surface sites (well probed by small molecules such as H_2O and CO) that appeared essentially unaffected by the organization at a longer range. Interestingly, once treated at 573 K crystalline surfaces appeared able to physisorb multilayers of water in a larger extent that the amorphous ones.

As an extension of this research, a comparative study of the amorphous and crystalline surfaces of nanohydroxyapatites in interaction with larger molecules, such as polypeptide and small proteins, will be carried out. Actually, this interaction should involve a multi-sites adsorption, which could then possibly be sensitive to the long range surface structure.

Acknowledgements

Y.S and M.I are recipients of a fellowships from Compagnia di San Paolo and Regione Piemonte, respectively. This research was carried out in the frame of PRIN project 2006062335, call 2006-2008. The activity carried out by M.I. was supported by the research project “Nanoparticelle multifunzionali per la terapia dei carcinomi: studi in vitro e in vivo in modelli sperimentali” funded by Regione Piemonte (Ricerca Sanitaria Finalizzata 2009). Prof. S. Coluccia (University of Torino) is kindly acknowledged for fruitful discussions.

.

.

Supporting Information Available. (1) XRD patterns, (2) IR spectra of HA-am and HA-cry exchanged with D2O and then outgassed at b.t, (3) example of data elaboration for the extraction of the signals due to adsorbed H2O, (4) plot of the integrated intensity of νOH vs. δH2O for HA-am and HA-cry, (5) IR spectra of HA-am in the νOH, δH2O and carbonate νCO regions, (6) IR spectra, in the δH2O and carbonate νCO regions of HA-am outgassed at increasing temperature and then contacted with 20 mbar H2O, (7) IR spectra of HA-am and HA-cry stepwise outgassed at increasing temperature and then contacted with 20 mbar H2O, outgassed at b.t., exchanged with D2O and outgassed at b.t.

References

[1] Castner, D.; Ratner, B. *Surf. Sci.* **2002,** *500*, 28–60.

[2] Kasemo, B. *Surf. Sci.* **2002,** *500*, 656–677.

[3] Tirrell, M.; Kokkoli, E.; Biesalski, M. *Surf. Sci.* **2002,** *500*, 61–83.

[4] Hermansson, M., *Coll. Surf. B: Biointerfaces* **1999**, *14*, 105-112.

[5] Wilson, C.; Clegg, R.; Leavesley, D.; Pearcy, M. *Tissue Eng.* **2005,** *11*, 1–18.

[6] E.A. Vogler In *Water in Biomaterials Surface Science*; Morra, M.; Ed., J. Wiley & Sons: Chichester, 2001.

[7] Dorozhkin, S.V. *Materials* **2009**, *2*, 1975-2045, and references therein.

[8] Zeitler, T.; Cormack, A. *J. Cryst. Growth* **2006**, *294*, 96–102.

[9] Pereira, M.; Jones, J.; Hench L. *Adv. Appl. Ceram.* **2005**, *104*, 35–42.

[10] LeGeros, R. *Chem. Rev.* **2008**, *108*, 4742–4753.

[11] Roveri, N.; Palazzo, B. In *Tissue, Cell and Organ Engineering*; Kumar, C.R., Ed.; J. Wiley & Sons: Chichester, 2006.

[12] Kandori, K.; Fudo, A.; Ishikawa T. *Colloids Surf., B* **2002**, *24*, 145–149.

[13] Capriotti, L.A.; Beebe, Jr., T.P.; Schneider, J.P. *J. Am. Chem. Soc.* **2007**, *129*, 5281-5287.

[14] Corno, M.; Rimola, A.; Bolis, V.; Ugliengo, P. *Phys. Chem. Chem. Phys*. **2010**, *12*, 6309-6329, and references therein.

[15] Robinson, R. A. *J. Bone Joint Surg*. **1952**, *34A*, 389–434.

[16] Lowenstam, H. A.; Weiner, S. *On Biomineralizalion*, Oxford University Press: New York, 1989.

[17] a) Webster, T.; Siegel, R.; Bizios, R. *Biomat*. **1999**, *20*, 1221–1227; b) Webster, T.; Ergun, C.; Doremus, R.; Siegel, R.; Bizios, R. *Biomat*. **2000**, *21*, 1803–1810; c) Webster, T.; Ergun, C.; Doremus, R.; Siegel, R.; Bizios, R. *Biomat*. **2001**, *22*, 1327–1333.

[18] Rinnerthaler, S.; Roschger, P.; Jakob, F.; Nader, A.; Klaushofer, K; Fratzl, P. *Calcif. Tissue Int.* **1999**, *64*, 422-426.

[19] Žižak, I.; Paris, O.; Roshger, P.; Bernstorff, S.; Amenitsch, H.; Klaushofer, K.; Fratzl, P. *J. Appl. Cryst.* **2000**, *33*, 820-823.

[20] Celotti, G.; Tampieri, A.; Sprio, S.; Landi, E.; Bertinetti, L.; Martra, G.; Ducati, C. *J. Mater. Sci.: Mater. Med.*, **2006**, *17*, 1079–1087.

[21] Isobe, T.; Nakamura, S.; Nemoto, R.; Senna, M.; Sfihi, H. *J. Phys. Chem B* **2002,** *106*, 5169–5176.

[22] Cazalbou, S.; Combes, C.; Eichert, D.; Ray, C. *J. Mater. Chem.*, **2004,** *14*, 2148–2153.

[23] Jaeger, C.; Welzel, T.; Meyer-Zaika, W.; Epple, M. *Magn. Reson. Chem.*, **2006,** *44*, 573–580.

[24] Bertinetti, L.; Tampieri, A.; Landi, E.; Ducati, C.; Midgley, P.; Coluccia S.; Martra, G. *J. Phys. Chem. C* **2007,** *111*, 4027–4035.

[25] Barheine, S.; Hayakawa, S.; Osaka, A.; Jaeger, C. *Chem. Mater.* **2009**, *21*, 3102–3109.

[26] Jaeger, C.; Groom, N.S.; Bowe, E.A.; Horner, A.; Davies, M.E.; Murray, R.C.; Duer, M.J. *Chem. Mater.* **2005**, *17*, 3059-3061.

[27] Bertinetti, L.; Drouet, C.; Combes, C.; Rey, C.; Tampieri, A.; Coluccia, S.; Martra, G. *Langmuir* **2009**, *25*, 5647–5654.

[28] Iafisco, M.; Palazzo, B.; Marchetti, M.; Margiotta, N.; Ostuni, R.; Natile, G.; Morpurgo, M.; Gandin, V.; Marzano, C.; Roveri, N. *J. Mater. Chem*. **2009**, *19*, 8385-8392.

[29] Klug, H.P.; Alexander, L.E. In *X-ray Diffraction Procedures for polycrystalline and amorphous materials*, J. Wiley & Sons: Chichester, 1974.

[30] Meldrum, A.; Wang, L.; Ewing, R. *Am. Mineral.*, **1997**, *82*, 858–869.

[31] Wang, L.; Wang, S.; Ewing, R.; Meldrum, A.; Birtcher, R.; Provencio, P.; Weber W.; Matzke, H. *Mater. Sci. Eng., A* **2000**, *286*, 72–80.

[32] LeGeros, R.; LeGeros J.; Trautz, O. *Dev. Appl. Spectros.* **1970**, *7B*, 3–12.

[33] Rheman, I.; Bonfield, W. *J. Mater. Sci.: Mater. Med.* **1997**, *8*, 1–4

[34] Landi, E.; Celotti, G.; Logriscino, G.; Tampieri, A. *J. Eur. Ceram. Soc.* **2003**, *23*, 2931–2937.

[35] Ishikawa, T.; Teramachi, A.; Tanaka, H.; Yasukawa, A.; Kandori K. Langmuir **2000**, *16*, 10221–10226.

[36] Corno M.; Busco, C.; Bolis, V.; Tosoni, S.; Ugliengo, P. *Langmuir* **2009**, *25*, 2188–2198.

[37] Hadjiivanov, K.; Vayssilov, G. *Adv. Catal.* **2002**, *47*, 307–511.

[38] Pekunov, Y.; Chakarova, K.; Hadjiivanov, K. *Mater. Sci. Eng., C* **2009**, *29*, 1178–1181.

[39] DeNoyer, L.K.; Dodd, J.G. In *Handbook of Vibrational Spectroscopy*; Chalmers, J.M., Griffiths P.R., Eds.; J. Wiley & Sons: Chichester, 2002; Vol. 3, p. 2173

Table 1. Codes, compositional features (Ca/P; carbonate content), specific surface area (SSABET), average size of crystal domains (along the [0,0,2] and [3,1,0] directions) and degree of crystallinity of the two materials.

Material	**Ca/P (mol)**	**Carbonate species (wt%)**	**SSA_{BET} ($m^2 \cdot g^{-1}$)**	**D_{002} * (nm)**	**D_{310} * (nm)**	**Degree of crystallinity**
HA-am	1.64	2	78±4	35 ± 8	10 ± 3	70% ± 3
HA-cry	1.65	1	68±4	51 ± 7	24 ± 3	83% ± 4

***** calculated applying the Scherrer equation

Table 2. Relative integrated intensity (I) of the νOH (3750-2500 cm-1 superposition of contributions due to hydroxy groups and H2O molecules) and δH2O (1800-1550 cm-1) bands (spectra in Fig. S3B) due to surface hydration species of HA-am and HA-cry in contact with 20 mbar H2O and outgassed at b.t. for 60 min. The integrated area of δH2O measured for HA-cry outgassed at b.t. was assumed as unity.

	Samples in contact with 20 mbar H_2O			**Samples outgassed at b.t.**		
	I νOH	*I* δH_2O	*I* νOH / *I* δH_2O	*I* νOH	*I* δH_2O	*I* νOH / *I* δH_2O
HA-am	75.9	3.5	21.7	33.5	1.2	27.9
HA-cry	67.6	3.2	21.1	22.4	1	22.4

Table 3. Amount of H2O molecules adsorbed per nm2 on HA-am and HA-cry in the presence of 20 mbar H2O vapour and after subsequent outgassing at b.t. for 120 min.

Entry	Surface hydration condition	HA-am	HA-cry
		materials thermally untreated	
		$H_2O \cdot nm^{-2}$	$H_2O \cdot nm^{-2}$
1	Multilayers resulting from the contact with 20 mbar of H_2O vapor	13.5±1.4	12.2±1.2
2	H_2O molecules left coordinated to surface cations by outgassing at b.t	4.5±0.5	3.7±0.5
		materials outgassed at 573 K and then rehydrated	
3	Multilayers resulting from the contact with 20 mbar of H_2O vapor	8.7±1.0	10.9±1.0
4	H_2O molecules left coordinated to surface cations by outgassing at b.t	2.0±0.3	2.0±0.3

Figure Captions

Figure 1. TEM image representative of the size and morphology of: A) HA-am and B) HA-cry particles. Original magnification: 80k×.

Figure 2. High resolution TEM image of a portion of a HA-am particle (main panel, left), related FT and zoomed view of the two enframed A', A'' border regions (right panels). Original magnification: 800k×.

Figure 3. High resolution TEM image of a portion of two HA-cry particles (panels A and B), related FT (right, bottom). Panels A', A'': zoomed view of two enframed border regions in panel A. Original magnification: 800k×.

Figure 4. IR spectra of: A) HA-am, and B) HA-cry. In both panels lettering is as follows: a) in the presence of 20 mbar H_2O; b) after 60 min. outgassing at b.t; c) after exchange with D_2O and subsequent 60 min outgassing at b.t. Insets: zoomed views of δ_{H2O} and carbonates ν_{CO} regions.

Figure 5. IR spectra of HA-cry in: A) νOH, B) δH_2O and C) carbonate νCO regions. In all sections lettering is as follows: samples outgassed for 60 min at: a) beam temperature, b) 373, c) 403, d) 433, e) 473, f) 523, g) 573 K. Spectra a'-g' were obtained by contacting the sample outgassed at the corresponding temperatures with D_2O vapour (20 mbar) and then outgassed for 60 min. at beam temperature.

Figure 6. Relative amount of H_2O molecules left adsorbed on HA-am (orange) and HA-cry (green) after outgassing at increasing temperature, with respect to the materials outgassed at beam temperature (100%). The evaluation was carried out on the basis of the integrated intensities of the δH_2O band in the IR spectra in Figure 5B (HA-cry) and Figure S5B (HA-am).

Figure 7. Plot of the surface hydration level attained on HA-am (orange) and HA-cry (green) outgassed at increasing temperature and then contacted with H_2O, with respect to the untreated materials (100%). Section A: water left adsorbed after outgassing at beam temperature. Section B: in the presence of 20 mbar H_2O. The evaluation was carried out on the basis of the integrated intensities of the δH_2O band in IR spectra in Supporting Information, Figure S7.

Figure 8. IR spectra of CO adsorbed at ca. 100 K on HA-am outgassed at 403 K (section A) and 573 K (section A') and on HA-cry outgassed at 433 (section B) and 573 K (section B'). Lettering is in the sense of decreasing CO pressure, from a) 25 mbar (blue) to j) outgassing for 1 min (red). Spectra are reported after subtraction of the spectrum of the materials outgassed at the corresponding temperatures before CO adsorption.

Figure 9. Second derivative of the spectra of CO adsorbed at 100 K on HA-am and HA-cry. Sections and lettering are as in Figure 8. Note that here the sense of decreasing CO coverage is now from the bottom (blue) to the top (red).

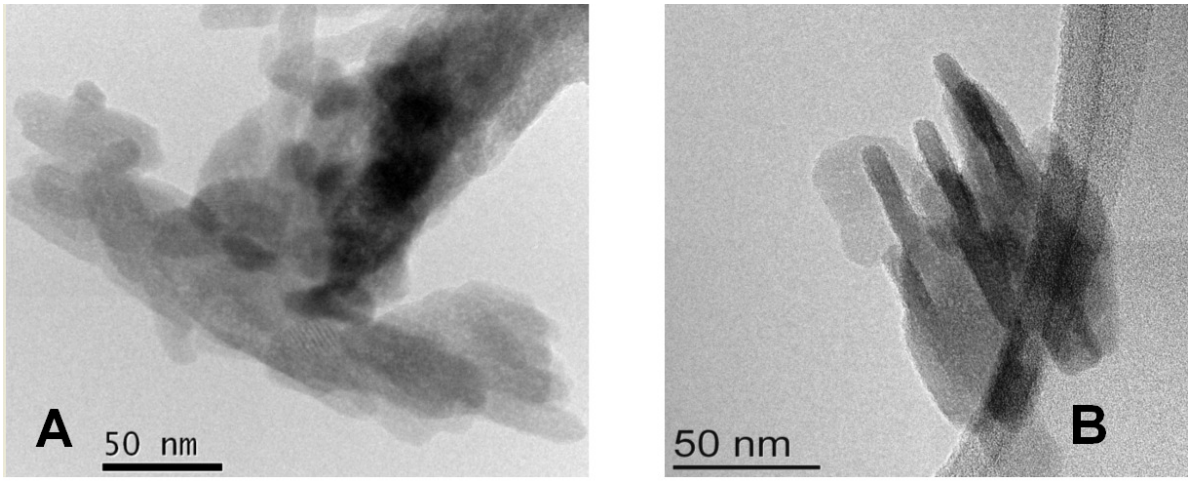

Figure 1

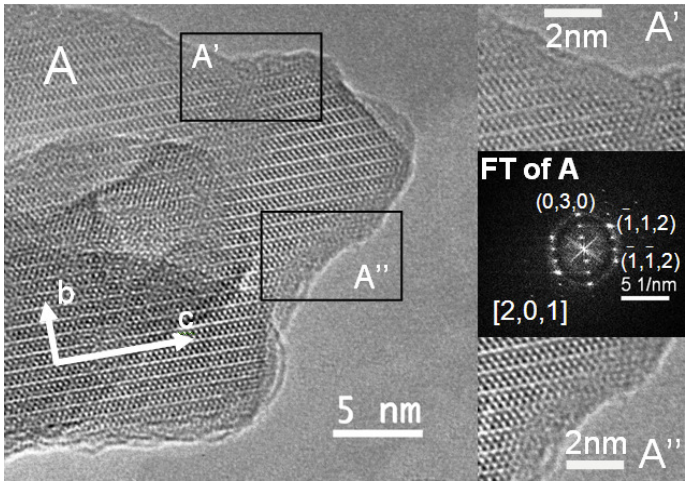

Figure 2

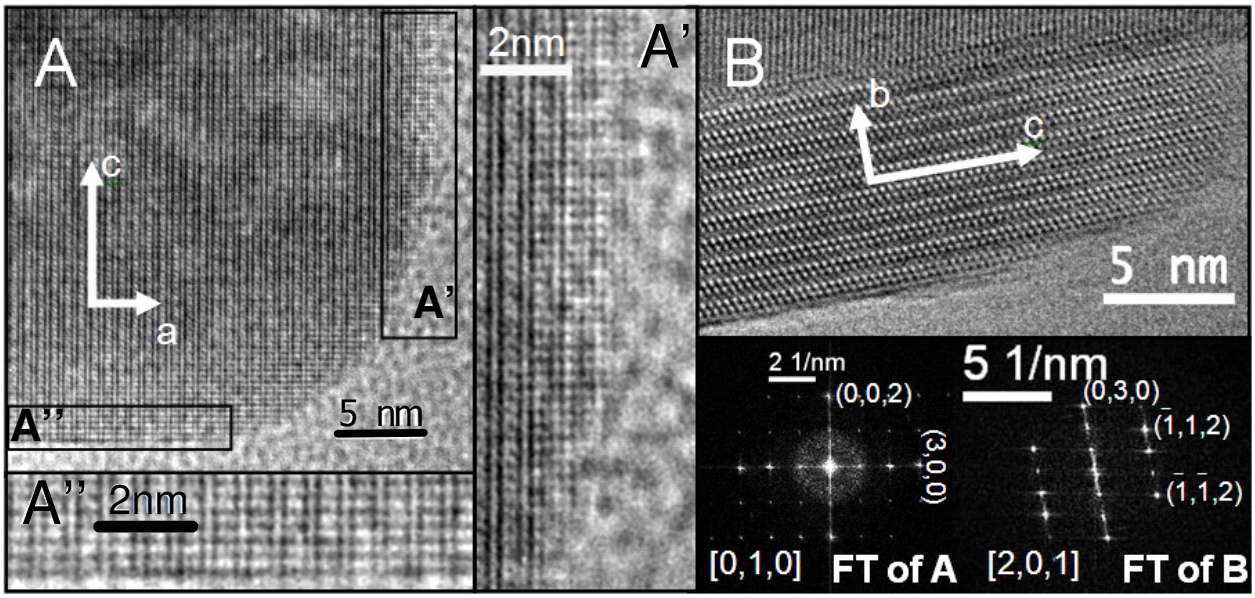

Figure 3

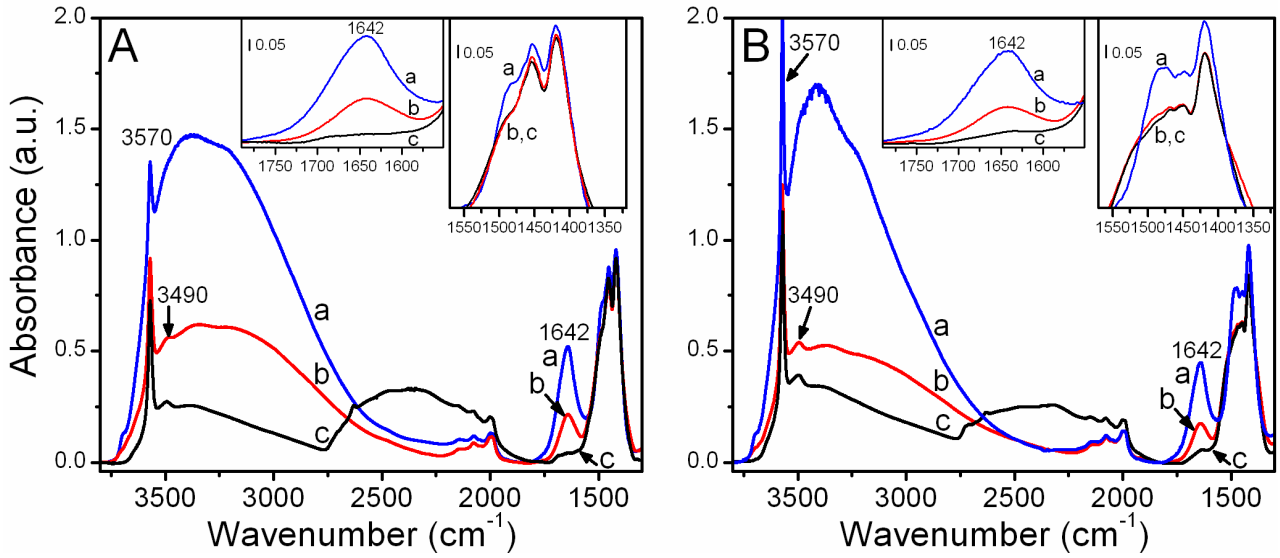

Figure 4

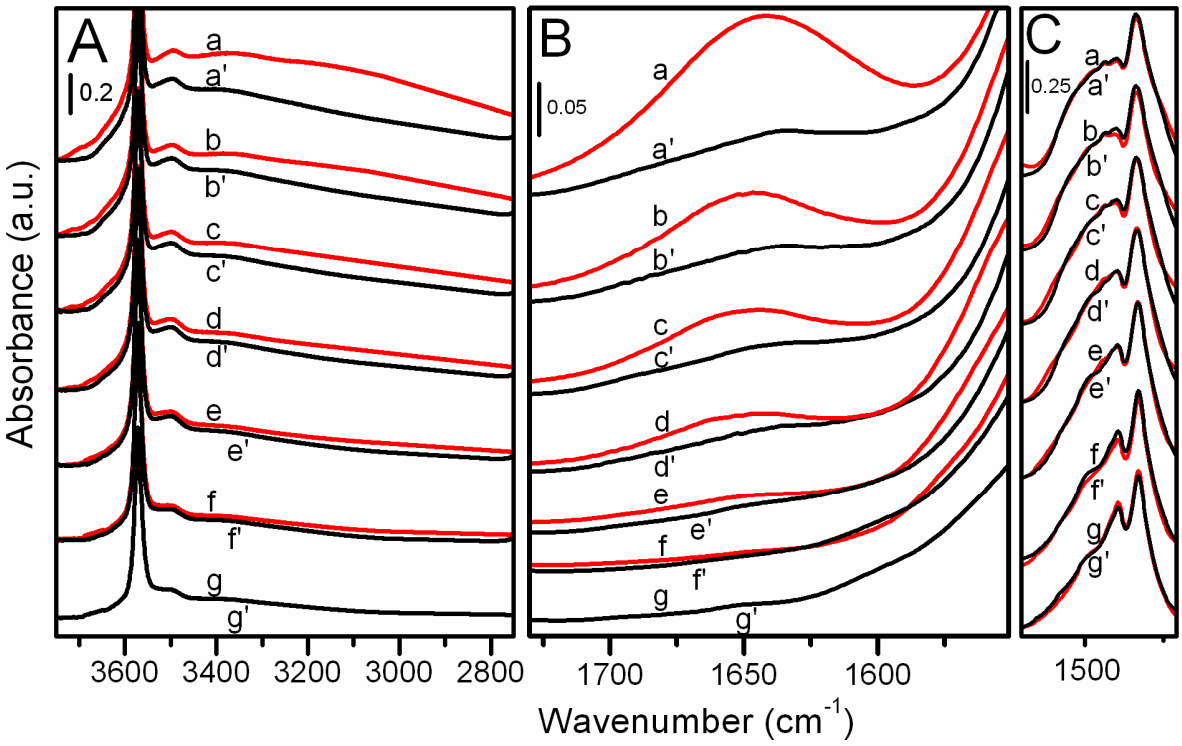

Figure 5

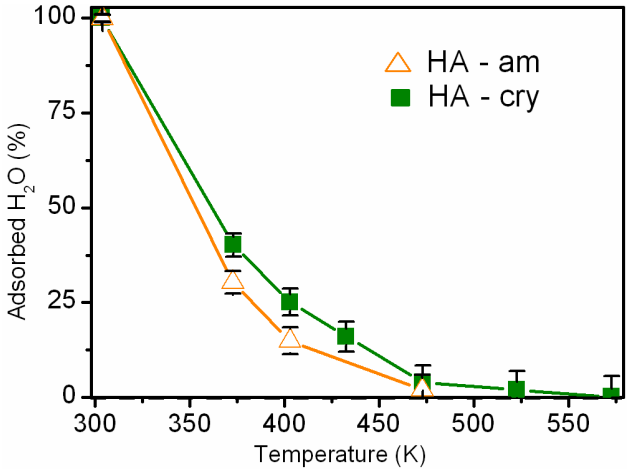

Figure 6

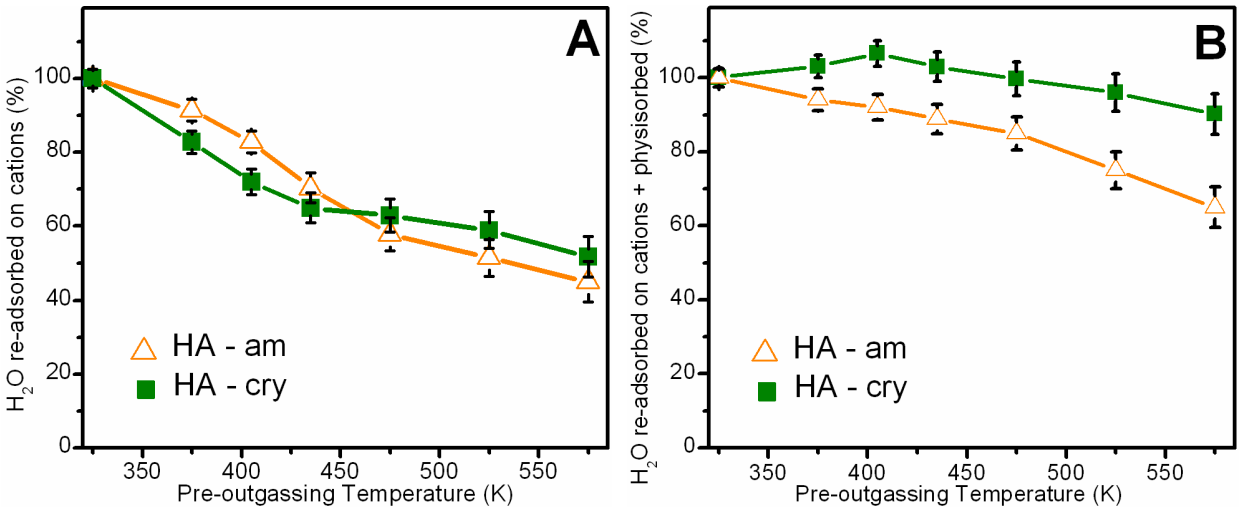

Figure 7

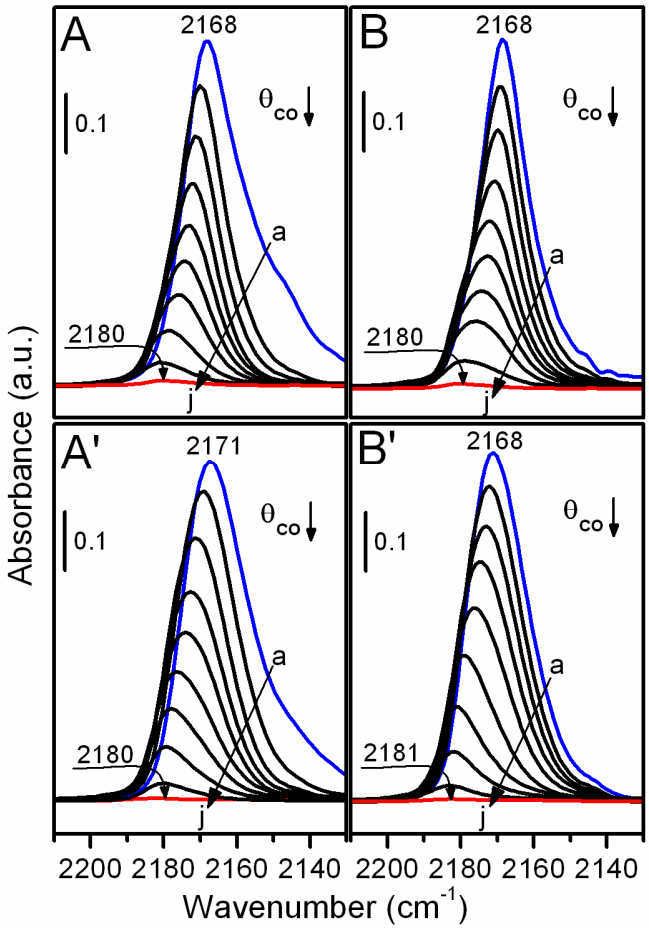

Figure 8

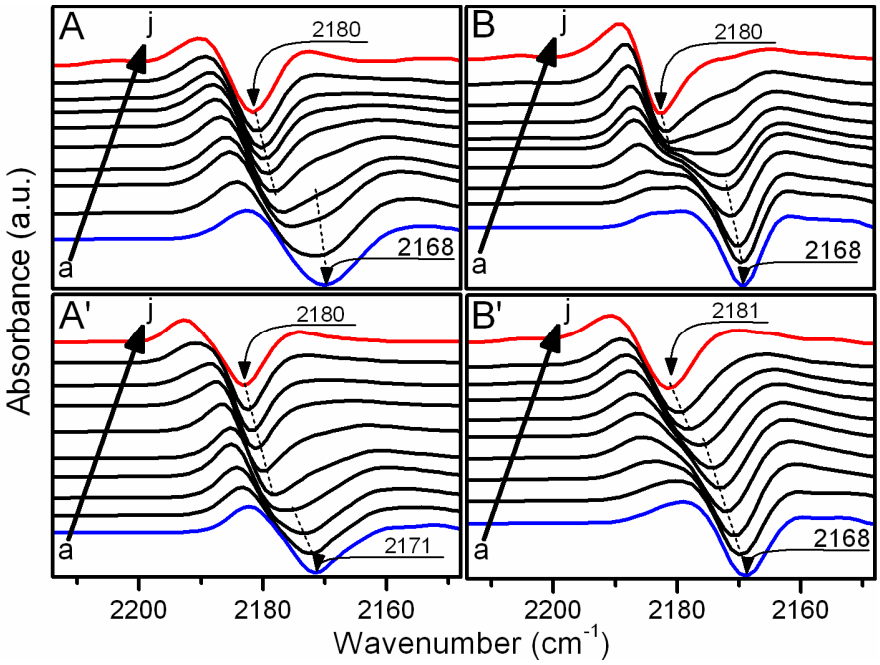

Figure 9

SYNOPSIS TOC

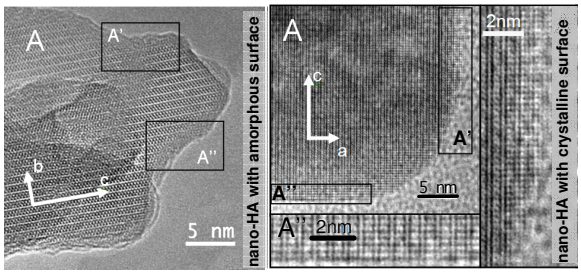

.